Available online at www.sciencedirect.com

ScienceDirect

Advances in Space Research 53 (2014) 1623–1633

ADVANCES IN SPACE RESEARCH (a COSPAR publication)

www.elsevier.com/locate/asr

Sensing snow height and surface temperature variations in Greenland from GPS reflected signals

Shuanggen Jin [a,*], Nasser Najibi [a,b]

[a] Shanghai Astronomical Observatory, Chinese Academy of Sciences, Shanghai 200030, China
[b] University of Chinese Academy of Sciences, Beijing 100049, China

Received 29 January 2014; accepted 3 March 2014
Available online 12 March 2014

Abstract

The *in situ* measurements of snow surface temperature (SST) and snow height (SH) are very difficult with high costs, particularly in Greenland Ice Sheet (GrIS). Since the snow depth variations coupling with surface temperature are related to GPS multipath, it is possible to estimate the snow depth and surface air temperature variations by incorporating GPS-Reflectometry (GPS-R). In this paper, the reflected signals from ground GPS receivers are used to sense the SST and SH variations based on the thermophysical behavior and variations of snow layer from April to June 2010 at SMM1 site and from March to December 2010 at MARG site in Greenland. The results show that the mean daily changes in the ionospheric geometrical-free linear combination (GPS-L4) of dual-frequency GPS signals are related to daily SST and SH variations. The nonparametric bootstrapping model in direct (forward) and inverse models are developed and applied to estimate the SST and SH variations. The mean biases of SST and SH estimates are 0.18 °C and 0.23 m at SMM1 site, respectively, and 3.8 °C and 0.13 m at MARG site, respectively.

Keywords: GPS-L4; Snow surface temperature; Snow height; Nonparametric bootstrapping model

1. Introduction

The continental ice sheets are frozen with volume changes related to the temperature and snowfall, which affect and are affected by the changes of Earth's climate. It also plays a significant role in the study of global and regional water cycle and mass energy balance (Jin et al., 2013). For example, the melting ice sheets and snow in Antarctic and Greenland are causing sea level rise with input fresh water from continental glaciers due to human-induced global warming (Rignot and Kanagaratnam, 2006; Rignot et al., 2011). Therefore, it is important to accurately estimate the ice sheets volume variations in very cold regions, like Greenland and Antarctica. Although the Greenland Ice Sheet (GrIS) is the second largest glacier in the world after Lambert Glacier located in East Antarctica (Diamond, 1960), it has an important impact on global sea level changes (Krabill et al., 2000; Cogley, 2004). Moreover, the dynamic GrISs reacts to the changes in the boundary conditions (Fausto et al., 2009).

The snow height (SH) and snow surface temperature (SST) dominate the climate change and hydrologic cycle as well as the energy exchange between the terrestrial surface, snowpack and the atmosphere. SH and SST are traditionally measured by special *in situ* instruments and sensors, however, it is very difficult to monitor global high temporal–spatial snow depth and near surface air temperature variations due to high costs and hard labor intensity (Li et al., 2013). Furthermore, when the precipitation reaches the

* Corresponding author at: Shanghai Astronomical Observatory, Chinese Academy of Sciences, Shanghai 200030, China. Tel.: +86 21 34775292.
E-mail addresses: sgjin@shao.ac.cn, sg.jin@yahoo.com (S. Jin).

http://dx.doi.org/10.1016/j.asr.2014.03.005
0273-1177/

ground surface, it begins to form as snow in the high atmosphere. These snowflakes form in above layers of atmosphere where the air temperature is less than 0 °C and start to fall toward the Earth's surface as snow. If the falling snow passes through the freezing level into the warmer air layer or arrives at snow surface with higher temperature than snowflake itself, it would be melt to the rain or runoff before reaching the snow surface. In addition, SST is also related to the snow melting and snow accumulating as well as the formation (Dreyfus et al., 2010).

Nowadays, the GPS reflected signals with the dual-frequencies on the frozen water (e.g. snowpack, ice caps, glaciers, etc.) allow us to detect the reflected surface characteristics (Martin-Neira, 1993; Elosegui et al., 1995; Hannah, 2001; Jin and Komjathy, 2010; Jacobson, 2010; Jin et al., 2010, 2011; Larson and Nievinski, 2012). Ozeki and Heki (2012) showed the snow depth retrieved from the geometry free linear combination of GPS observations in Japan. In this paper, SST and SH variations are estimated and investigated using the multipath signals as GPS-L4 fluctuations from ground GPS receivers in Greenland, where wide snowpack, ice sheets and permafrost are available in the whole days of year. Moreover, the thermophysical behavior of snow layer with SH, SST and GPS-L4 variations are assessed and nonparametric bootstrapping model is developed in both direct and inverse modeling. Some results on the SST and SH variations from the inverse of bootstrap model are compared with the meteorological data. Finally, conclusions are given as well as discussions.

2. Theory and methodology

2.1. Thermophysical behavior of snow

The snow-covered surface has a dynamic reaction to the climate change in different regions (Bavay et al., 2013), depending mostly on the length of snow falling and melting seasons in addition to the characteristics of snow (grain size, density, etc.) and the geomorphology of area (Rödder and Kneisel, 2012). The key to assess the SST–SH changes is referring to thermophysical properties of snow as a non-isolated medium. The flux of heat at one dimension is given by Fourier equation as (Armstrong and Braun, 2008):

$$F = -k_{eff}\frac{\partial T}{\partial d} \tag{1}$$

where F is the flux of heat, k_{eff} is the effective thermal conductivity, T is the temperature degree (in Kelvin) and d is the special coordinate along the direction of flow. Considering the snow layer as thermal advective–diffuse heat

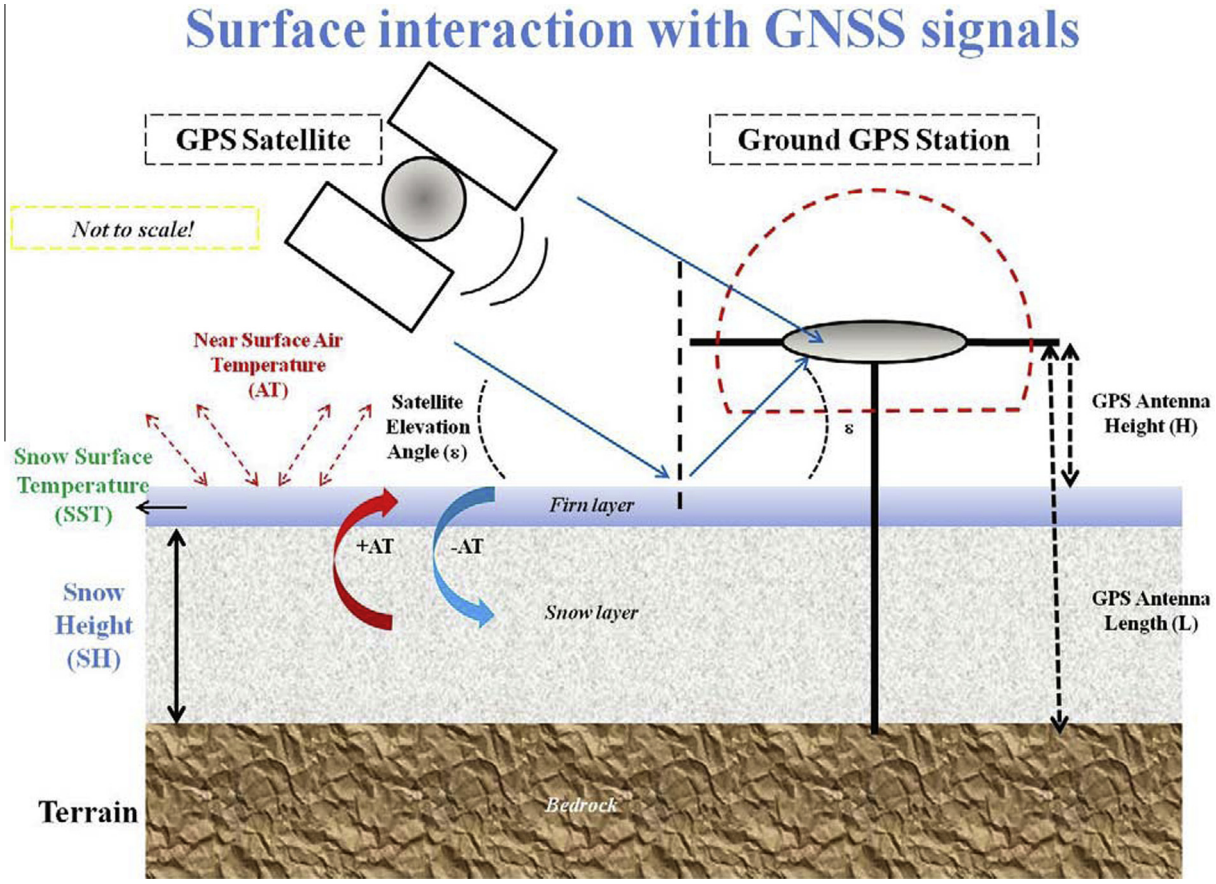

Fig. 1. Snow height and snow surface temperature interactions with GPS signals.

transfer equilibrium, the heat exchange can be occurred at the special time span (t) in a special direction coordinate as follow:

$$\rho_s c_{p,s} \frac{\partial T}{\partial t} + \phi \rho_k c_{p,k} v_k \frac{\partial T}{\partial d} = \frac{\partial}{\partial d}\left[k_{eff} \frac{\partial T}{\partial x}\right] + q \quad (2)$$

where T, d and k_{eff} are the same definitions in Eq. (1), ρ_s is the density of normal snow (127 kg/m^3), v_k is the flow velocity of fluid k (according to the layer of snow if it includes air ($k = a$) or water ($k = l$), and $c_{p,s}$ is the specific heat coefficient of snow, which depends on snow density and the specific heat coefficient of water ($c_{p,l} = 4217$ J kg^{-1} K^{-1}), specific heat coefficient of air ($c_{p,a} = 1005$ J kg^{-1} K^{-1}) and specific heat coefficient of ice ($c_{p,i} = 2114$ J kg^{-1} K^{-1}) (Fukusako, 1990), q and ϕ denote the heat source (mostly near surface air temperature) and the ratio of heat flow in the pure snow, respectively.

According to Eqs. (1) and (2), the flow of heat in the snow layer is a function of thermodynamic parameters of not only the snow but also the water, ice and air, which exist in the snow layer. If there is no water, ice or air in the snow and the snow is considered as a completed shaped snow (idealistic snow layer), the heat transfer is more straightforward rather than Eqs. (1) and (2). Thus, the Eqs. (1) and (2) will be simplified as the flow of heat conduction in the snow medium given as follow (Albert and McGilvary, 1992):

$$H = -L_{ik} S \quad (3)$$

where H stands for the thermal source term, S stands for the melt or freeze phase change and L_{ik} defines as the following two terms on occasion:

- in snow accumulation; L_{ik} as L_{il} is the latent heat of fusion,
- in snow melting; L_{ik} as L_{iv} is the latent heat of sublimation.

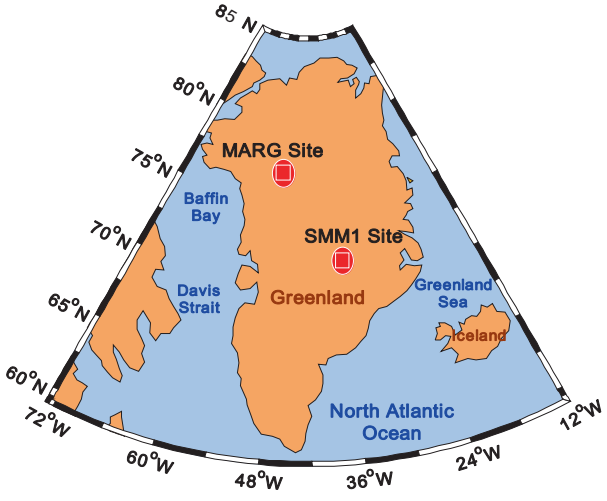

Fig. 2. Locations of co-located GPS and meteorological stations in Greenland.

It should be noted that if the fluid (air or water) flows through the snow layer, the heat transport will take place as a function of advective and diffusive processes. In this study, we assume that the snow layer is a complete snow without any water, air or even any other extraneous elements inside it (e.g. vegetation layer, floral substances, etc.). From Eq. (3), the decrease in snow depth is certainly resulted from the increase in the near surface air temperature and vice versa, It should note valid in the dynamic climate conditions.

2.2. GPS reflected signals from carrier phase and pseudorange

GPS reflected signals would result in the multipath, which are the errors for GPS navigation and positioning. It is highly dependent on the environment around the GPS receiver and not well cancelled by the differencing techniques, since it is a highly localized phenomenon and depends on the type of antenna and the tracking loop algorithms of the receiver. However, the GPS reflected signals can be considered as a useful signal to identify the characteristics of surrounding GPS's receiver environment (Jin et al., 2011). The GPS multipath can be extracted using the ionospheric free geometrical linear combination as follows:

$$\mathrm{GPS} - L4 = \Phi_{\mathrm{IF}} = -\frac{f_1^2}{f_1^2 - f_2^2} \times \Phi_1 + \frac{f_2^2}{f_1^2 - f_2^2} \times \Phi_2 \quad (4)$$

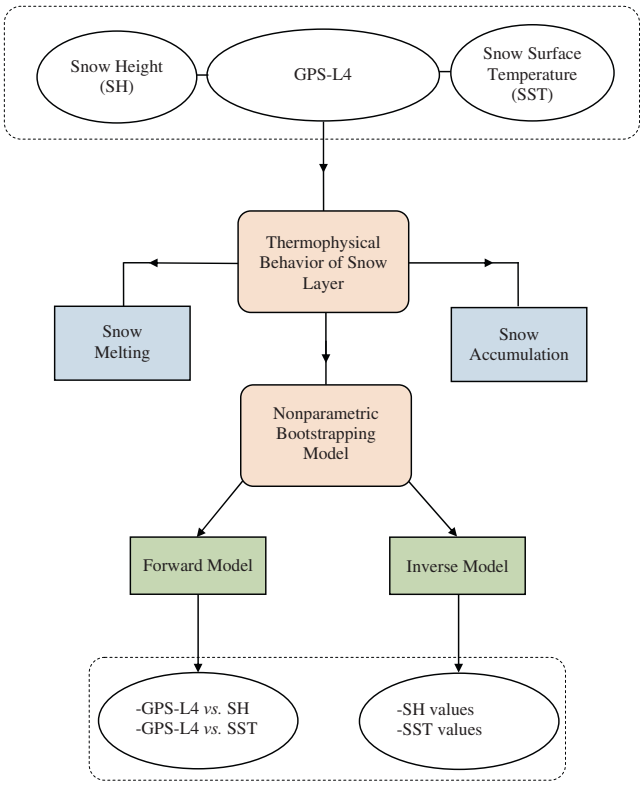

Fig. 3. The proposed flowchart and modules in this study.

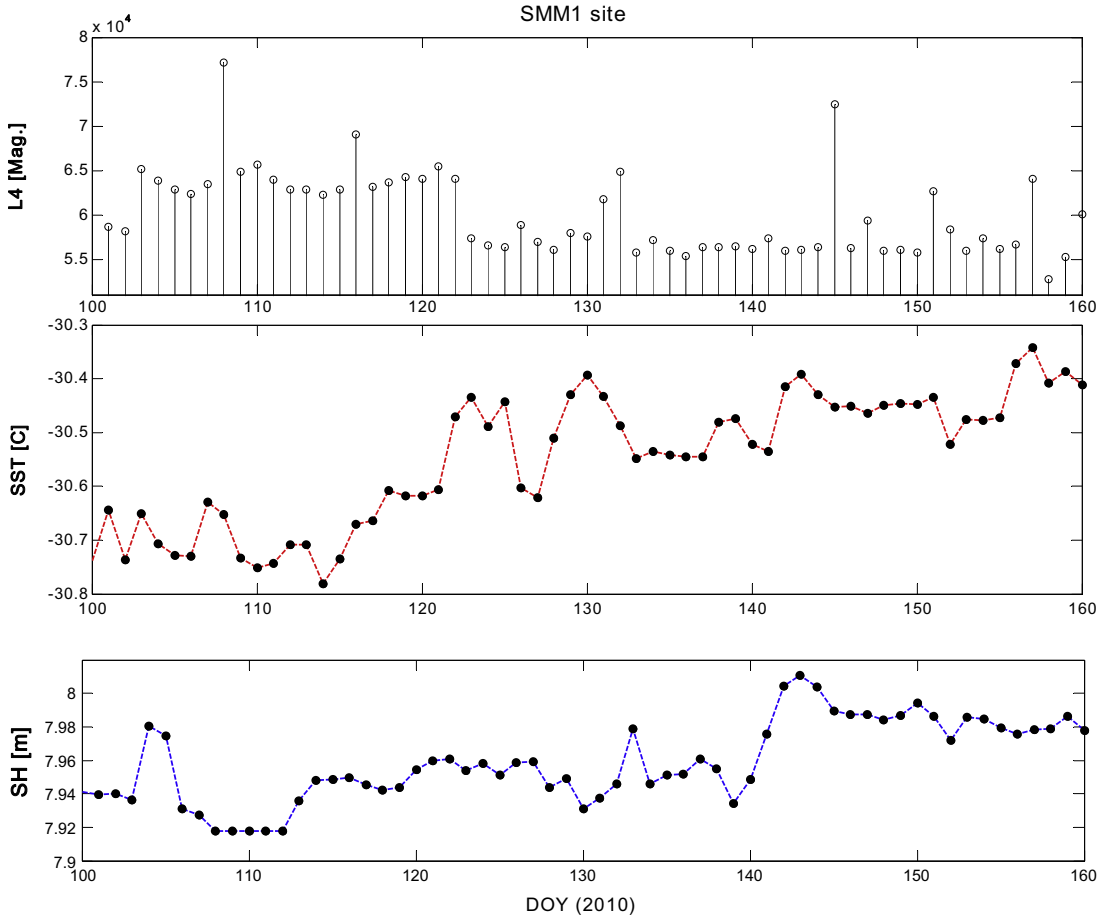

Fig. 4. GPS-L4, SST and SH variations at SMM1 site in Greenland.

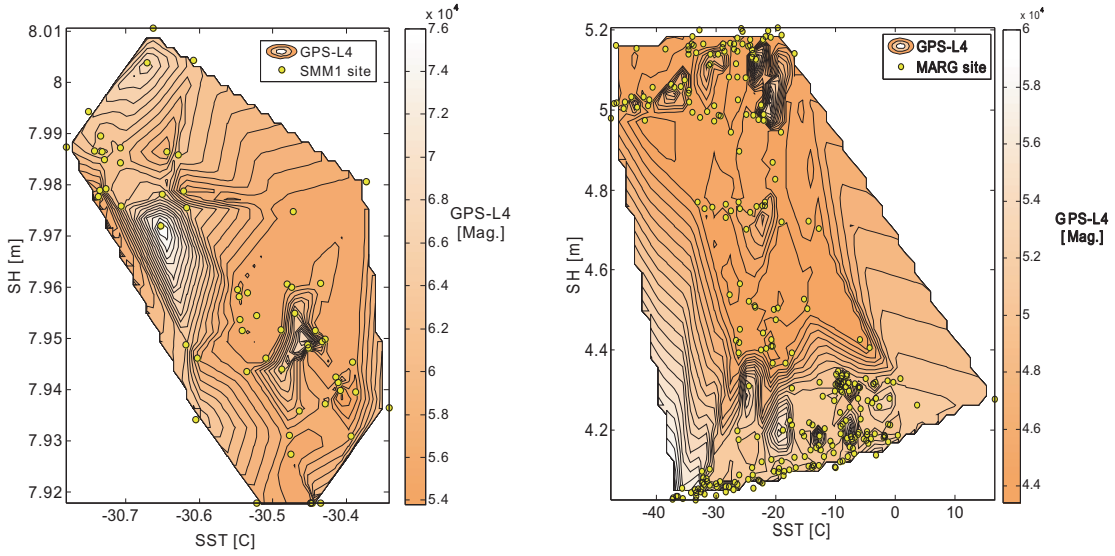

Fig. 5. Thermophysical trend of snow at SMM1 (left) and MARG (right) sites with SH, SST and GPS-L4 variation.

where Φ_{IF} is ionospheric free geometrical linear combination (GPS-L4), f_1 and f_2 are GPS frequencies ($f_1 = 1575.42$ MHz, $f_2 = 1227.60$ MHz), and Φ_1 and Φ_2 are the GPS dual-frequency carrier phase signals.

2.3. Connections of GPS-L4, SH and SST changes

Elosegui et al. (1995) and Leick (2004) firstly introduced the mechanism of GPS reflected signals through multipath

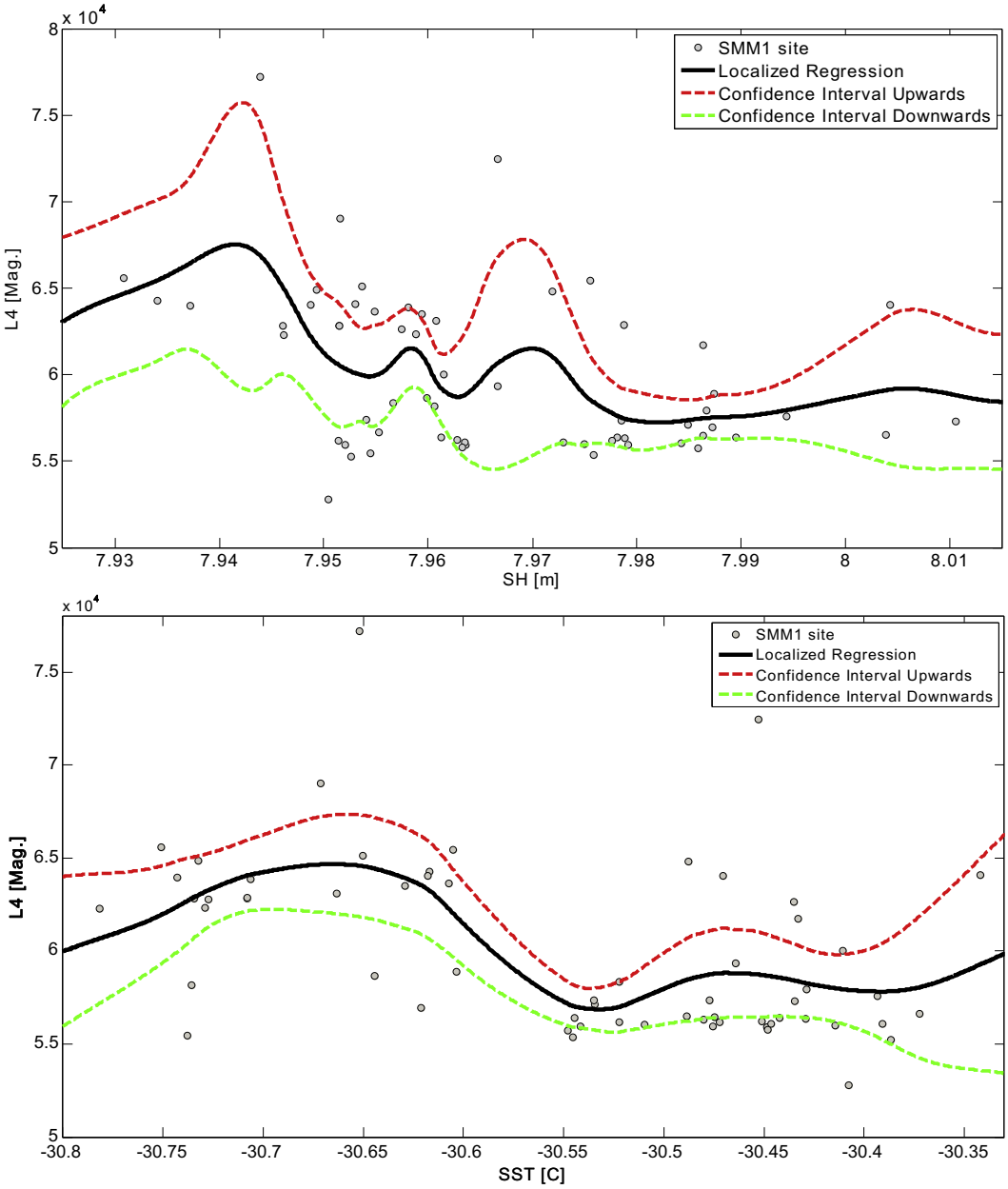

Fig. 6. Nonparametric bootstrap model (black) of GPS-L4 variations vs. SH (up) and SST (down) at SMM1 site. The two confidence intervals for bootstrapping model are presented as upper dot (red) and down dot (green). (For interpretation of the references to color in this figure legend, the reader is referred to the web version of this article.)

contribution to the signal phase ($\delta\Phi$). Fig. 1 shows the snow height and snow surface temperature interactions with GPS signals. The contribution of SH to the GPS reflected signals was given by Najibi and Jin (2013) as follows:

$$\delta\Phi(\alpha, N, H) = \tan^{-1}\frac{\alpha\sin(NH)}{1+\alpha\cos(NH)} \tag{5}$$

where H is the height of GPS antenna, α is the reflected surface characteristic and $N = 4\pi\lambda^{-1}\sin(\varepsilon)$ where $\lambda = cf^{-1}$ (c is the speed of the light) and f is the corresponding GPS dual-frequency signals ($L_1 = 1575.42$, $L_2 = 1227.60$ MHz). In order to investigate the variation of GPS-L4 with respect to SH, the variability of GPS-L4 with respect to the changes of the GPS antenna height for GPS dual-frequency signals ($\lambda_1 = 0.1902$ and $\lambda_2 = 0.2442$ m) is derived as:

$$\begin{aligned}\frac{dL4(\varepsilon,\alpha,H,f)}{dH} &\cong \frac{d\delta\Phi(\varepsilon,\alpha,H,\lambda)}{dH}\\ &= -\frac{f_1^2}{f_1^2-f_2^2}\times\frac{d\delta\Phi}{dH}(\alpha,\varepsilon,H,\lambda_1)\\ &\quad+\frac{f_2^2}{f_1^2-f_2^2}\times\frac{d\delta\Phi}{dH}(\alpha,\varepsilon,H,\lambda_2)\end{aligned} \tag{6}$$

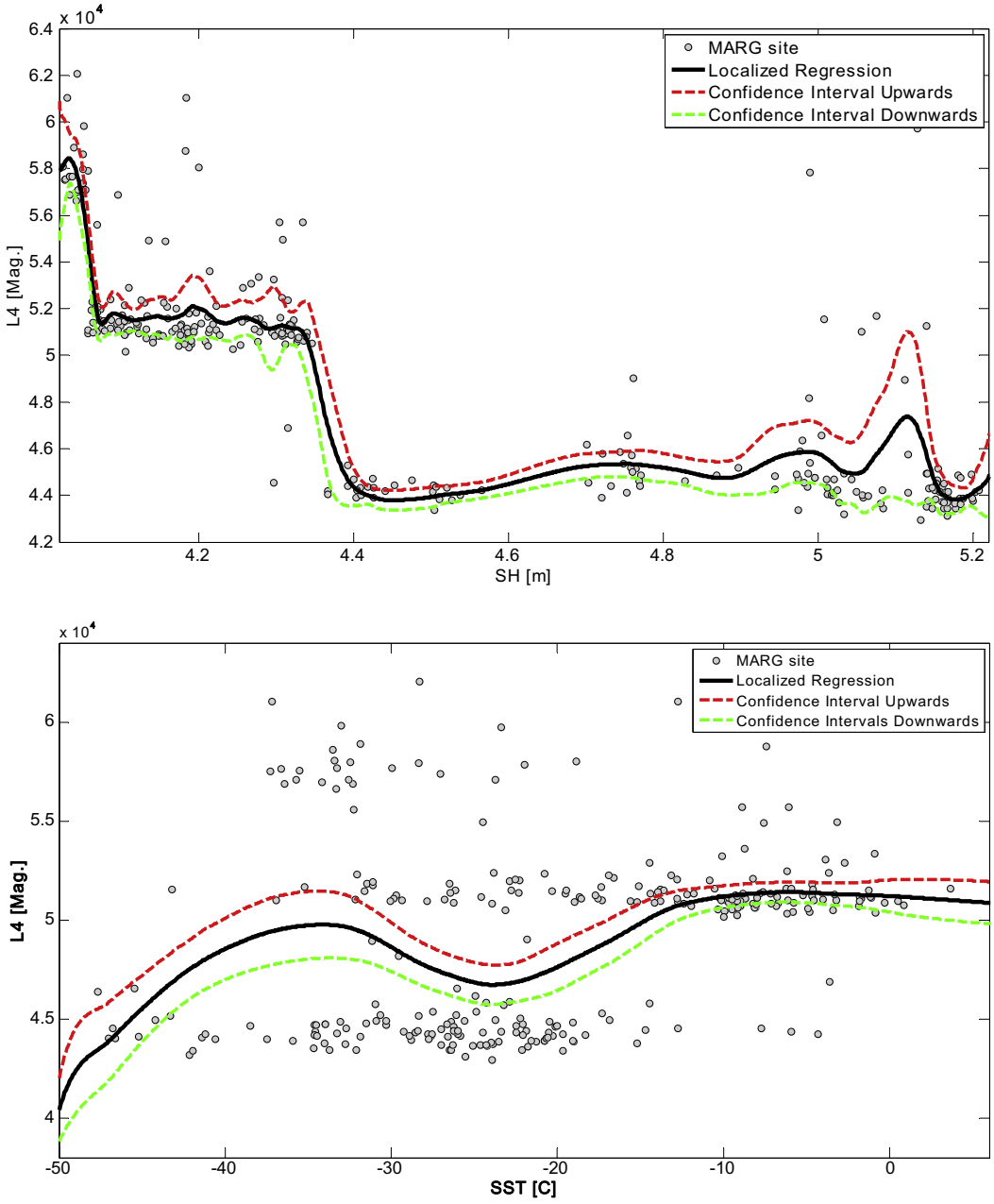

Fig. 7. Nonparametric bootstrap model (black) of GPS-L4 variations vs. SH (up) and SST (down) at MARG site.

where $\frac{d\delta\Phi}{dH}$ is the changes of GPS reflected signals with respect to H, and f_1 and f_2 are L_1 and L_2 corresponding GPS signal frequencies.

2.4. Non-parametric bootstrapping model

The bootstrapping model was firstly introduced by Efron (1979) as an alternative approach to deal with the convoluted data distribution models. The proposed bootstrapping model builds a sampling distribution for a statistic estimator by resampling the available data, which performs empirical distribution function (EDF) and probability density function (PDF) of nonparametric bootstrapping (Efron and Tibshirani, 1993). Although EDF and PDF are the most critical functions in construction of the model, particularly for the inverse direction of bootstrapping, but EDF estimates the unknown cumulative distribution function (CDF) by giving equal probabilities to the original values (here GPS-L4 variations) and each output value (here SST and SH), while each one is independently modeled. Therefore the bootstrap modeled output's trend is an empirical normalized sample with replacement from the original trend. There are many advantageous with using bootstrapping model. Firstly, it does not require any distributional assumptions and even the bootstrap can provide more accurate inferences when

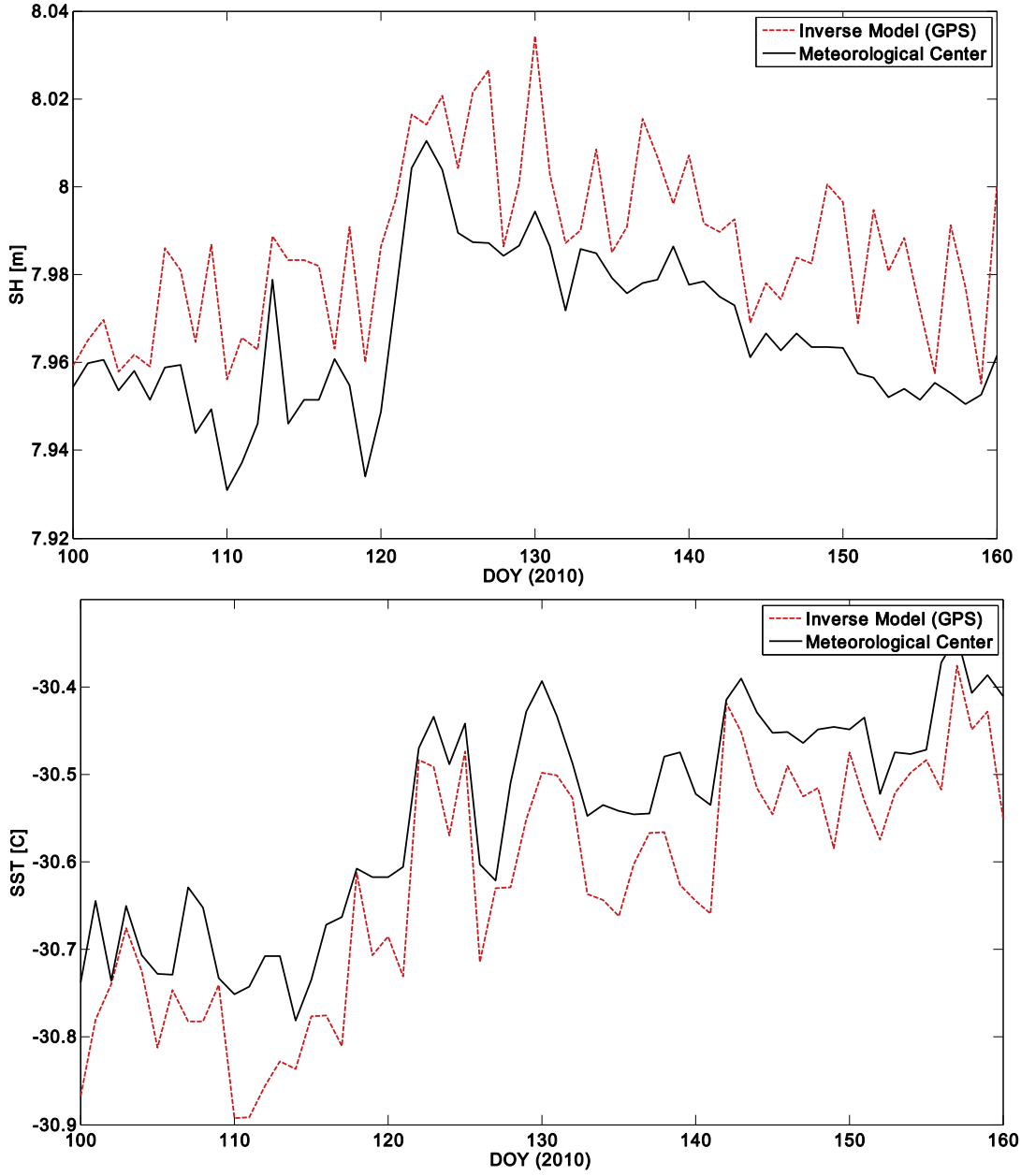

Fig. 8. Comparison of SH (up panel) and SST (down panel) from the inverse model of bootstrapping model (GPS-L4) and meteorological observations at SMM1 site.

the data are not well behaved uniquely in the entire span as well as when the sample size is small (Davison and Hinkley, 1997). Secondly, it is possible to apply the bootstrap to the statistics with sampling distributions that are difficult to derive even asymptotically. Besides, it is relatively simple to apply the bootstrap to complex data collection sorts (e.g. stratified and clustered samples). In this paper, the changes on SH and then on H are considered as the variability of GPS-L4 values with respect to H. Moreover, the connection between SST variations and SH (and then GPS-L4) are discussed through thermophysical behavior of snow layer in Section 2.3.

3. Observations and results

3.1. GPS observation data

Two GPS stations SMM1 (72.58°N and 38.46°W) and MARG (77.19°N and 65.69°W) with nearly two co-located Greenland Climate Network Automated Weather Stations (GC-Net-AWS) titled Summit (72.57°N and 38.50°W) and GITS (77.14°N and 61.04°W) sites are used (Fig. 2). SMM1 and MARG GPS sites equipped with a receiver type of AOA-BENCHMARK-ACT and AOA-BENCHMARK-ACT as well as antenna type of AOAD/M_B and

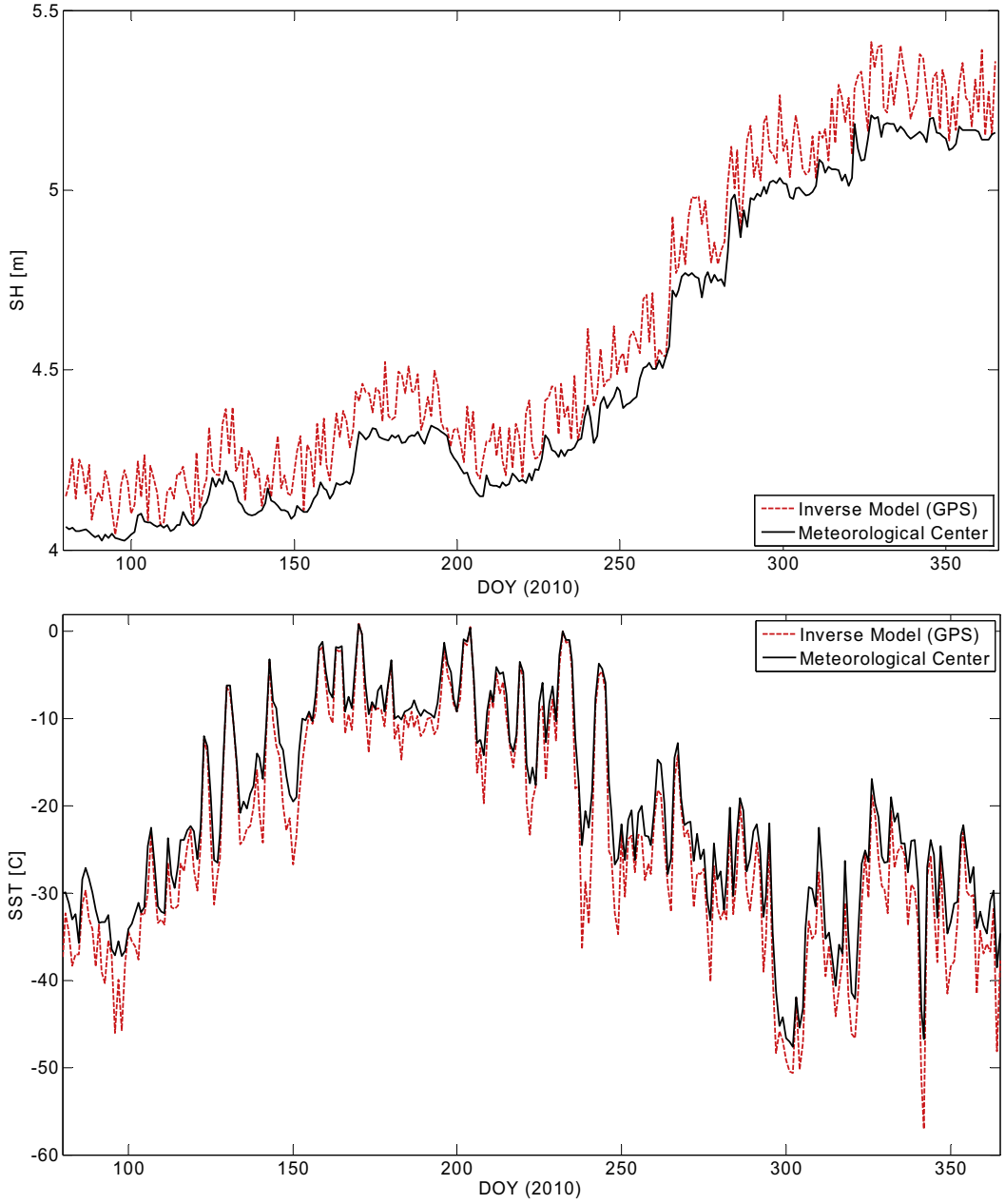

Fig. 9. Comparison of SH (up panel) and SST (down panel) from the inverse model of bootstrapping model (GPS-L4) and meteorological observations at MARG site.

TPSCR.G3, respectively. They can receive dual-frequency observations per 30 s continuously. The daily 2880-epoch observations for 32 satellites are used during 61 days from April 10 to June 9, 2010 at SMM1 and 286 days from March 21 to December 31, 2010 at MARG station. The average daily GPS-L4 values from all the feasible observed satellites observables at SMM1 and MARG stations are extracted and used for this study.

The hourly SST and SH measurements are observed at two co-located meteorological stations, which are a part of Greenland Climate Network Automated Weather Station (GC-NET-AWS) established by Cooperative Institute for Research in Environmental Sciences (CIRES), University of Colorado, Boulder, USA (Steffen et al., 1996). These meteorological stations' instruments are generally working based on World Meteorological Organization (WMO) standards. The mean daily SST (°C) and SH (m) values are obtained as average daily values.

3.2. Variability of GPS-L4, SST and SH

The general flowchart of estimating SST and SH variations is shown in Fig. 3. Although GPS-L4 daily value consists of many varying parameters, but GPS-L4 as multipath signals mostly varies due to variability of satellite elevation angle and GPS antenna height (Najibi and Jin, 2013). In

this study, since we did not restrict our GPS dual-frequency signals to specific satellite elevation angles, GPS-L4 values are mostly subjected to the GPS antenna height variations.

Table 1
Statistics of estimating SST and SH from GPS-L4 values.

Inverse model (GPS)			
Station	Days	Correlation coefficient	RMS
SST [°C]			
SMM1	61 (100–160)	−0.79	0.18
MARG	286 (080–365)	0.69	3.81
SH [m]			
SMM1	61 (100–160)	−0.77	0.23
MARG	286 (080–365)	−0.84	0.13

Consequently, the SH changes mostly caused by near surface air temperature variations around the GPS station may contribute to GPS-L4. Accordingly, the GPS-L4 value will be changed after snow melting or snow accumulation during a period time.

Fig. 4 shows variations of GPS-L4, SH and SST at SMM1 site from April 10 to June 9, 2010. The SST is about −30.7 °C and the GPS-L4 is equal to 6.5×10^4 Magnitude. When the SST is constant, the GPS-L4 values are stable. The SST variations affect on the SH values and then GPS reflected signals as GPS-L4. Similarly, SH variations are in consistent with GPS-L4 fluctuations in both SMM1 and MARG sites, particularly where the SH are

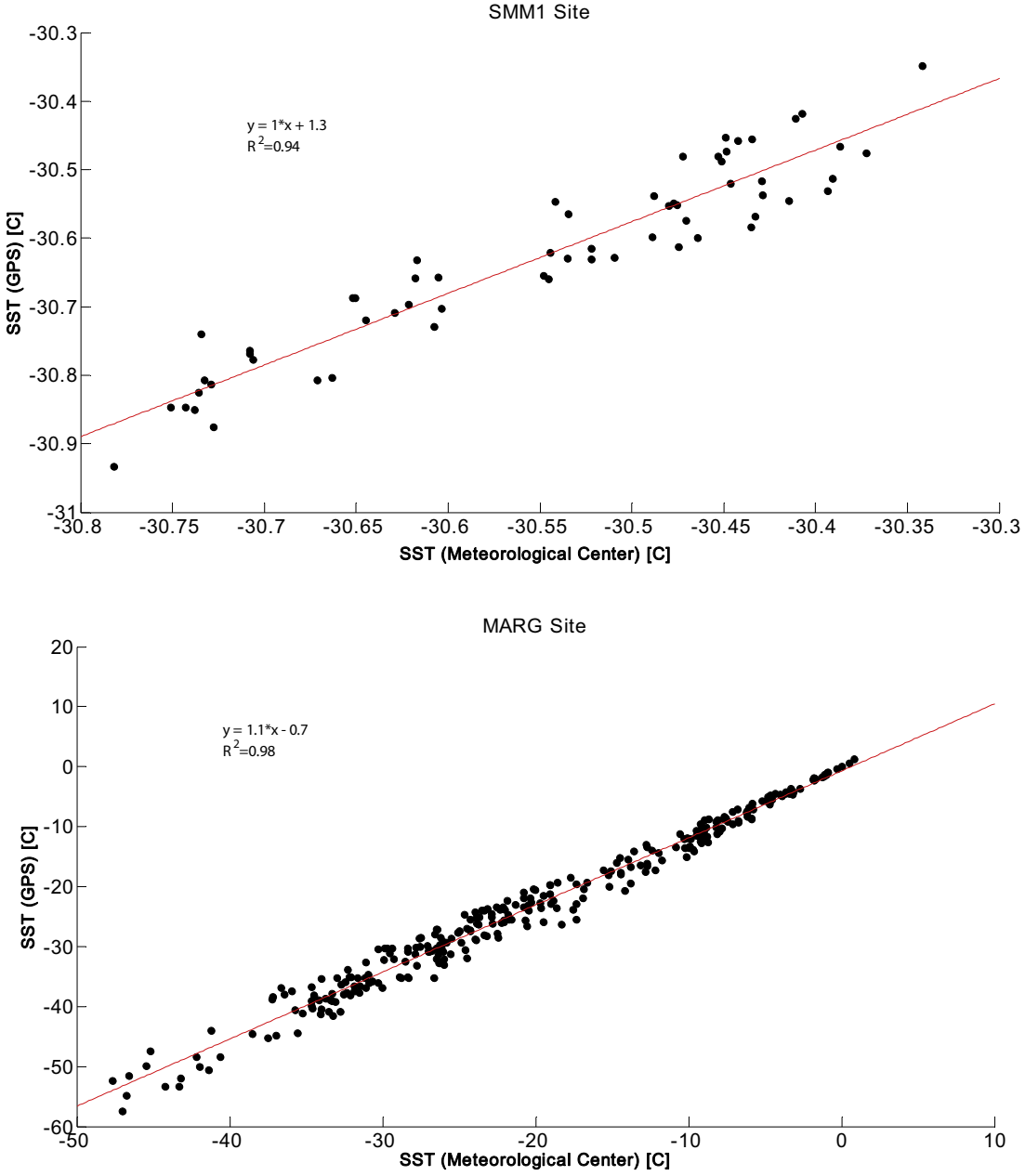

Fig. 10. SST from inverse model of bootstrapping model (GPS-L4) and meteorological observations at SMM1 (up panel) and MARG (down panel) sites.

increasing and the GPS-L4 values are decreasing continuously.

3.3. Responses of thermophysical properties of snow surface to SST variability

The variability of SST with respect to SH changes are presented in Fig. 5 for both SMM1 and MARG sites with GPS-L4 changes. While it is assumed that there is no any other fluids within the snow layers as well as complete snow, the distribution of SST vs. SH with the GPS-L4 values is satisfying the Eq. (3) based on the thermophysical responses of snow layers to the near surface air temperature variation. The decrease in SST would be resulted in the increase of SH values and vice versa. Meanwhile, the GPS-L4 values are changing continuously due to the changes of GPS reflected signals, which are originated from the caused phase shift in the GPS scattered signals. The interactions of SST and SH values and then on GPS-L4 ones can be clearly seen at both SMM1 and MARG sites.

3.4. Nonparametric bootstrapping model

In order to model the GPS-L4 and SST and SH variations in each specified time span, nonparametric modeling technique of bootstrapping method is proposed. In general, the bootstrapping constructs a sampling distribution for a statistic estimator by resampling from the data at hand. There are several forms of the bootstrap and additionally several other resampling methods, such as jackknifing, cross-validation, randomization tests and permutation tests (Chernick, 2011). In this study we use nonparametric bootstrapping modeling to estimate the sampling distribution of GPS-L4 vs. SST and SH variations without any assumptions. Besides, the bootstrapping model creates two confidence intervals, upwards and downwards, which are very sensitive to but not influenced directly by original scatters (Figs. 6 and 7).

Since there is no enough information about the type of measurements, the Monte Carlo simulation cannot be used (Efron and Tibshirani, 1993). The confidence interval in the bootstrapping model is a region with a high percentage of the total distribution relative to model parameters of interest. We used the confidence level of 68.3% and the region shape of lines for developing the bootstrapping model. In order to estimate the values of SST and SH from GPS-L4's variations at SMM1 and MARG GPS stations, the inverse model of bootstrapping model is assessed. Fig. 8 and Fig. 9 present the comparison of SST and SH from the inverse bootstrapping model and the meteorological centers (AWSs).

The mean bias of SST and SH are 0.18 °C and 0.23 m with corresponding Pearson correlation coefficient of −0.79 and −0.77 at SMM1 site, respectively and 3.8 °C and 0.13 m with Pearson correlation coefficient of 0.69 and −0.84 at MARG site, respectively. The model outputs of the proposed bootstrapping model has an acceptable mean bias (Table 1). More importantly, it is clearly seen in Fig. 10 that there is a good agreement between the estimated SST from the inverse of bootstrap model of GPS-L4 with the meteorological data at both SMM1 and MARG sites.

4. Conclusion and discussions

In this paper, the variations of SST and SH are estimated and investigated from GPS reflected signals at two GPS sites in Greenland during the year of 2010. The thermophysical performance of snow layer was taken into account for estimating the SST by means of GPS-L4 values during the snow accumulating and melting. The results show that the daily values in the GPS-L4 fluctuations are influenced homogenously by the daily SST and SH variations at SMM1 site during 61 days from April 10 to June 9, 2010 and at MARG site during 286 days from March 21 to December 31, 2010. Furthermore, the proposed nonparametric bootstrapping models in both direct (forward) and inverse model give relatively accurate estimates of daily SST and SH variations from GPS-L4. The mean bias for SST and SH are 0.18 °C and 0.23 m at SMM1 site, respectively, and 3.8 °C and 0.13 m at MARG site, respectively.

GPS reflected signals are valuable for the cryosphere and hydrological studies by measuring SST and SH. This will provide new opportunities of the current International GNSS Service (IGS) networks to estimate the climate system parameters, particularly in high latitudes. Here we demonstrated the SST and SH estimation from GPS reflected signals using the nonparametric bootstrapping model under the thermophysical behavior of an idealistic snow layer. In the future, it needs more field experiments and data to further investigate the SST and SH estimation from GPS reflected signals with considering various impacts and errors in different snow types and geographical latitudes.

Acknowledgments

This research is supported by the Main Direction Project of Chinese Academy of Sciences (Grant No. KJCX2-EW-T03), Shanghai Science and Technology Commission Project (Grant No. 12DZ2273300) and National Natural Science Foundation of China (NSFC) Project (Grant Nos. 11173050 and 11373059).

References

Albert, M.R., McGilvary, W.R., 1992. Thermal Effects due to air flow and vapor transport in dry snow. J. Glaciol. 38 (129), 273–281.

Armstrong, R.L., Brun, E., 2008. Snow and Climate: Physical Processes, Surface Energy Exchange and Modeling. Cambridge University Press, Cambridge, 222 p.

Bavaya, M., Grünewald, T., Lehning, M., 2013. Response of snow cover and runoff to climate change in high alpine catchments of Eastern Switzerland. Adv. Water Resour. 55 (2013), 4–16.

Chernick, M.R., 2011. Bootstrap Methods: A Guide for Practitioners and Researchers, second ed. John Wiley & Sons, New York, p. 400.

Cogley, J.G., 2004. Greenland accumulation: an error model. J. Geophys. Res. 109, D18101. http://dx.doi.org/10.1029/2003JD004449.

Davison, A.C., Hinkley, D.V., 1997. Bootstrap Methods and Their Application. Cambridge University Press, New York, 582 p.

Diamond, M., 1960. Air temperature and precipitation on the Greenland ice sheet. J. Glaciol. 3 (27), 558–567.

Dreyfusa, G.B., Jouzela, J., Benderb, M.L., Landaisa, A., Masson-Delmottea, V., Leuenbergerc, Markus, 2010. Firn processes and δ15N: potential for a gas-phase climate proxy. Quat. Sci. Rev. 29, 28–42.

Efron, B., Tibshirani, B., 1993. An Introduction to the Bootstrap. Chapman & Hall, London, UK, 436 p.

Efron, B., 1979. Bootstrap methods: another look at the jackknife. Ann. Stat. 7, 1–26.

Elosegui, P., Davis, J.L., Jaldehag, R.K., Johansson, J.M., Niell, A.E., Shapiro, B., 1995. Geodesy using the global positioning system: the effects of signal scattering. J. Geophys. Res. 100, 9921–9934.

Fausto, R.S., Ahlstrom, A.P., van As, D., Boggild, C.E., Johnsen, S.J., 2009. A new present day temperature parameterization for Greenland. J. Glaciol. 55 (189), 95–105.

Fukusako, S., 1990. Thermophysical properties of ice, snow, and sea ice. Int. J. Thermophys. 11 (2), 353–372. http://dx.doi.org/10.1007/BF01133567.

Hannah, B.M., 2001. Modeling and simulation of GPS multipath propagation (Ph.D. thesis). The Cooperative Centre for Satellite Systems, Queensland University of Technology, Australia.

Jacobson, M.D., 2010. Inferring snow water equivalent for a snow-covered ground reflector using GPS multipath signals. Remote Sens. 2, 2426–2441. http://dx.doi.org/10.3390/rs2102426.

Jin, S.G., Komjathy, A., 2010. GNSS reflectometry and remote sensing: new objectives and results. Adv. Space Res. 46 (2), 111–117. http://dx.doi.org/10.1016/j.asr.2010.01.014.

Jin, S.G., Feng, G.P., Gleason, S., 2011. Remote sensing using GNSS signals: current status and future directions. Adv. Space Res. 47 (10), 1645–1653. http://dx.doi.org/10.1016/j.asr.2011.01.036.

Jin, S.G., Luo, O.F., Ren, C., 2010. Effects of physical correlations on long-distance GPS positioning and zenith tropospheric delay estimates. Adv. Space Res. 46 (2), 190–195. http://dx.doi.org/10.1016/j.asr.2010.01.017.

Jin, S.G., van Dam, T., Wdowinski, S., 2013. Observing and understanding the Earth system variations from space geodesy. J. Geodyn. 72, 1–10. http://dx.doi.org/10.1016/j.jog.2013.08.001.

Krabill, W., Abdalati, W., Frederick, E., Manizade, S., Martin, C., Sonntag, J., Swift, R., Thomas, R., Wright, W., Yungel, J., 2000. Greenland ice sheet: high-elevation balance and peripheral thinning. Science 289 (5478), 428–430. http://dx.doi.org/10.1126/science.289.5478.428.

Larson, K.M., Nievinski, F.G., 2012. GPS snow sensing: results from the earth scope plate boundary observatory. GPS Solutions. http://dx.doi.org/10.1007/s10291-012-0259-7.

Leick, A., 2004. GPS Satellite Surveying, third ed. John Wiley & Sons Publisher, 435 p.

Li, Z.L., Tang, B.H., Wu, H., Ren, H., Yan, G., Wan, Z., Trigo, I.F., Sobrino, J.A., 2013. Satellite-derived land surface temperature: current status and perspectives. Remote Sens. Environ. 131, 14–37. http://dx.doi.org/10.1016/j.rse.2012.12.008.

Martin-Neira, M., 1993. A passive reflectometry and interferometry system: application to ocean altimetry. ESA J. 17, 331–355.

Najibi, N., Jin, S.G., 2013. Physical reflectivity and polarization characteristics for snow and ice-covered surfaces interacting with GPS signals. Remote Sens. 5 (8), 4006–4030. http://dx.doi.org/10.3390/rs5084006.

Ozeki, M., Heki, K., 2012. GPS snow depth meter with geometry-free linear combinations of carrier phases. J. Geod. 86 (3), 209–219. http://dx.doi.org/10.1007/s00190-011-0511-x.

Rignot, E., Kanagaratnam, P., 2006. Changes in the velocity structure of the Greenland ice sheet. Science 986, 311. http://dx.doi.org/10.1126/science.1121381.

Rignot, E., Velicogna, I., van den Broeke, M.R., Monaghan, A., Lenaerts, J., 2011. Acceleration of the contribution of the Greenland and Antarctic ice sheets to sea level rise. Geophys. Res. Lett. 38, L05503. http://dx.doi.org/10.1029/2011GL046583.

Rodder, R., Kneisel, C., 2012. Influence of snow cover and grain size on the ground thermal regime in the discontinuous permafrost zone. Swiss Alps Geomorphol. 175–176, 176–189.

Steffen, K., Box, J.E., Abdalati, W., 1996. Greenland climate network: GC-Net. In: Colbeck, S.C. (Ed.), CRREL 96–27 Special Report on Glaciers, Ice Sheets and Volcanoes, tribune to M. Meier, pp. 98–103.